Journal of Sound and Vibration 329 (2010) 700–720

Contents lists available at ScienceDirect

Journal of Sound and Vibration

journal homepage: www.elsevier.com/locate/jsvi

Study of a misaligned flexibly coupled shaft system having nonlinear bearings and cyclic coupling stiffness—Theoretical model and analysis

I. Redmond

Dynamic Analysis Unit, Saudi Aramco, R-99,Bldg. 9155, Dhahran 31311, Saudi Arabia

ARTICLE INFO

Article history:
Received 11 April 2009
Received in revised form
31 August 2009
Accepted 30 September 2009
Handling Editor: H. Ouyang
Available online 28 October 2009

ABSTRACT

A model which enables dynamic analysis of flexibly coupled misaligned shafts is presented. The model is setup to account for both angular and parallel misalignment in the presence of mass unbalance and incorporates a coupling having angular, torsional and axial flexibility. Among the important features is the ability to simulate both nonlinear bearing stiffness and coupling angular-stiffness anisotropy. The equations of motion are derived for the linear system, extended to include nonlinear bearing effects and subsequently transformed into non-dimensional form for general application. A series of numerical analyses are performed and the influence of important system parameters assessed thereby providing insight to the resulting static and dynamic forces and motions. Angular and parallel misalignments are shown to produce fundamentally different system response. It is found that the static preload induced by both types of misalignment can play a key role in producing complex vibration resulting from it's interaction with rotating-element anisotropy and bearing nonlinear properties. Bearing static forces are altered and rotating elements are subjected to alternating forces which could affect fatigue life. Bearing forces can be further modified by the application of transmitted torque. The potential for great variability in system response is shown to exist due to the participation of numerous influential variables.

1. Introduction

The presence of misalignment in coupled-shaft systems is a major reliability issue in present-day critical machinery applications, even though the practical procedures necessary to ensure acceptable alignment are well known [1]. The ability to clearly diagnose the presence of misalignment using vibration analysis can be vital in reducing costly machine unscheduled downtime. However, this can be a difficult task due to the complexity of the misalignment-vibration relationship. For instance, many publications cite the presence of a twice running speed vibration component as strong evidence of misalignment, yet field observations frequently contradict this. Indeed some studies not only reinforce the view that second-harmonic vibration need not be present but conclude that there is no unique misalignment-related vibration characteristic [2]. The evidence so far indicates that the form of the vibration resulting from misalignment is greatly dependent upon many factors including the extent and type of misalignment (i.e. parallel vs angular), coupling type, bearing type, transmitted-torque level, etc. This makes sense when one considers the possible numerous combinations of such influential parameters in a modern rotating equipment train and may go some way to explain the spectral variability

E-mail addresses: irvredmond@aol.co.uk

0022-460X/$ - see front matter © 2009 Elsevier Ltd. All rights reserved.
doi:10.1016/j.jsv.2009.09.039

Nomenclature

a shaft overhang dimension
A_1, A_2, A_3 system constants
c load torque constant
$[C]$ damping matrix
C_x, C_y, C_t, C_z damping constants (x and y lateral, torsional and axial)
D_x, D_y nonlinear bearing parameters
e mass eccentricity
F_{xa}, F_{ya} bearing static forces due to angular misalignment
F_{xp}, F_{yp} bearing static forces due to parallel misalignment
g gravitational constant
h dimension defining mass/inertia location on shaft
I_1, I_2 rotor polar moments of inertia
k_c coupling angular stiffness constant
$k_{c\alpha}$, $k_{c\beta}$ coupling angular stiffness
k_n, k_{nx}, k_{ny} bearing nonlinear-stiffness coefficient
k_x, k_y support stiffness
k_c, k_t, k_z coupling stiffness constants ($k_t \approx I_2 \cdot \omega_{nt}^2$)
$[K]$ stiffness matrix
L shaft length, Lagrangian
m rotor mass
m_x, m_y bearing nonlinear-stiffness exponents
$[M]$ mass/inertia matrix
$M_{N\alpha}, M_{N\beta}, M_{N\phi}$ nonlinear-bearing reaction moments
n_p no. of coupling bolt-pairs or stiffness-defects
$\{q\}, \{\dot{q}\}, \{\ddot{q}\}$ generalised displacement, velocity and acceleration
$\{Q_i\}$, $\{Q_{Di}\}$, $\{Q_{Tdi}\}$, $\{Q_{TIi}\}$ generalised force vectors
R_1, R_2 rotor radii of gyration
t time
T kinetic energy
T_d drive torque
T_L load torque
u mass unbalance
V potential energy
x_1, y_1, x_2, y_2 Rotor2 displacements at bearings 1 and 2
z_1 shaft axial displacement at coupling
α shaft angular displacement about x-axis
$\dot{\alpha}$ shaft angular velocity about x-axis
$\ddot{\alpha}$ shaft angular acceleration about x-axis
α_0 initial angular misalignment about x-axis
β shaft angular displacement about y-axis
$\dot{\beta}$ shaft angular velocity about y-axis
$\ddot{\beta}$ shaft angular acceleration about y-axis
β_0 initial angular misalignment about y-axis
δ shaft parallel offset (misalignment)
λ_i coupling stiffness anisotropy reference angle
ω_{nx} lateral natural frequency, x-direction, $[(k_x(a^2 + L^2) + k_c)/h^{*2}mL^2]^{1/2}$
ω_{ny} lateral natural frequency, y-direction, $[(k_y(a^2 + L^2) + k_c)/h^{*2}mL^2]^{1/2}$
ω_{nz} axial natural frequency, z-direction, $[k_z/m]^{1/2}$
ω_{nt} torsional natural frequency, $[k_t/I_2]^{1/2}$
ω_x, ω_y, ω_z angular velocities—rotor 1
ω_{xx}, ω_{yy}, ω_{zz} angular velocities—rotor 2
ϕ rotor 2 rotational displacement
Ψ rotor 1 rotational displacement
$\dot{\phi}$ rotor 2 rotational velocity
τ rotor 2 coupling hub skew-angle
Θ parallel misalignment reference angle

Dimensionless parameters

a^* shaft overhang, $a^*=a/L$
$[C^*]$ damping matrix
f_x frequency ratio, $f_x = \omega_{nx}/\omega_{ny}$
f_t frequency ratio, $f_t = \omega_{nt}/\omega_{ny}$
f_z frequency ratio, $f_z = \omega_{nz}/\omega_{ny}$
F^*_{xa}, F^*_{ya} Brg. static forces due to angular misalignment=$F_{x,ya}/\alpha_0 k_y L$
F^*_{xp}, F^*_{yp} Brg. static forces due to parallel misalignment=$F_{x,yp}/k_y\delta$
g^* gravity moment, $g^* = g/\omega_{ny}^2 L$
h^* mass location parameter, $h^*=h/L$
k_1 stiffness ratio, $k_1 = k_x/k_y$
k^*_c coupling stiffness, $k^*_c = k_c/k_Y L^2$
$k^*_{c\alpha}$ coupling stiffness, $k^*_{c\alpha} = k^*_c \cdot [1 + \sum_{i=1}^{i=N} a_i \cdot \cos(i\phi + \lambda_i)]$
$k^*_{c\beta}$ coupling stiffness, $k^*_{c\beta} = k^*_c \cdot [1 + \sum_{i=1}^{i=N} a_i \cdot \sin(i\phi + \lambda_i)]$
k^*_{nx}, k^*_{ny} nonlinear stiffness coefficient
k_v coupling stiffness anisotropy parameter
$[K^*]$ stiffness matrix
$[M^*]$ mass/inertia matrix
$M^*_{N\alpha}, M^*_{N\beta}, M^*_{N\phi}$ dimensionless nonlinear bearing reaction moments
p parallel offset, $p = \delta/L$
$\{q^*\}, \{\dot{q}^*\}, \{\ddot{q}^*\}$ generalised response vectors
r_1, r_2 radii of gyration, $r_1=R_1/L$; $r_2=R_2/L$
T^*_d drive torque, $T^*_d = T_d/mL^2\omega^2_{ny}$
T^*_L load torque, $T^*_L = T_L/mL^2\omega^2_{ny}$
x^*_2, y^*_2 shaft displacements at bearing 2; for parallel misalignment, $x^*_2 = x_2/\delta$; $y^*_2 = y_2/\delta$; for angular misalignment, $x^*_2 = x_2/\beta_o L$; $y^*_2 = y_2/\beta_o L$
z^*_1 rotor 2 axial displacement
$\dot{\alpha}^*$ shaft angular velocity about x-axis
$\ddot{\alpha}^*$ shaft angular acceleration about x-axis
$\dot{\beta}^*$ shaft angular velocity about y-axis
$\ddot{\beta}^*$ shaft angular acceleration about y-axis
ζ_x damping ratio, $\zeta_x = C_x/2m\omega_{nx}$
ζ_y damping ratio, $\zeta_y = C_y/2m\omega_{ny}$
ζ_z damping ratio, $\zeta_z = C_z/2m\omega_{nz}$
ζ_t damping ratio, $\zeta_t = C_t/2m\omega_{nt}$

Abbreviations

RS running speed

observed in the field. Given these facts it is surprising that, in comparison to other areas of vibration study, the topic of shaft-misalignment has received relatively little attention.

Ref. [3] is one of the earliest publications to present equations describing the forces resulting from a misaligned flexible-element coupling. Dewell and Mitchell [4] analysed a disk-coupling and based on measurements proposed vibration monitoring of twice and four times per-rev harmonics as a means of diagnosing misalignment. A good summary of the main publications related to design, analysis and experimental study of flexible-element couplings was provided by Xu and Marangoni [5] who later performed a theoretical study on a misaligned shaft system [6]. Even-order vibration was predicted by assuming driven shaft speed fluctuations resulting from the 'Hooke's-Joint' effect. The authors' provided experimental data to support their theory, in a companion paper [7].

A series of theoretical studies [8–11] were presented based on the assumption that system $1\times$ and $2\times$ excitation forces are produced by mass unbalance interaction with shaft speed fluctuations resulting from the Hooke's Joint effect. Parallel and angular misalignment were considered and rotor systems with rigid [8] and flexible [9] couplings were investigated. It was concluded that shaft misalignment had little effect on $1\times$ vibration response while it greatly influenced $2\times$ response. The same approach was adopted in [10] where second-harmonic response due to misalignment was shown to be more dominant than that resulting from a shaft crack. Prabhakar et al. [11] investigated the use of wavelets as a condition monitoring tool to identify misalignment from transient data. It was reported that using this approach a number of sub-critical speeds could be identified when misalignment was present. Armugam et al. [12] analysed a misaligned two-stage turbine by representing the coupling reaction forces as a half-sinusoid function, thereby leading to $2\times$ excitation. It was found that angular misalignment produced a response dominated by even numbered harmonics with amplitude proportional to transmitted torque.

A combined theoretical and experimental study of a misaligned rotor on ball bearings [13] showed that the natural frequency was increased and the vibration response decreased, in the direction of the misalignment while only running speed vibration was observed. Jackson [14] cited examples of industrial machines where misalignment produced substantial second-harmonic response due to the nonlinear properties of oil-film bearings. Hili et al. [15] presented a simple theoretical model for angular misalignment which showed vibration components at $1\times$ and $2\times$ running speed and at the system natural frequency. The reduction of bearing reactions with increasing coupling flexibility was also demonstrated. Hussain and Redmond [16] analysed misaligned rigidly coupled rotors and concluded that parallel misalignment is a source of both lateral and torsional excitations. Lees [17–19] and Redmond [20] separately investigated linear misaligned shaft systems and reported that parallel misalignment can lead to torsional fluctuations which could produce a significant $2\times$ vibration response in the absence of coupling kinematic excitations and component nonlinearities. Redmond [20] reported that, in the case of parallel misalignment, support stiffness asymmetry was an important factor in accentuating 2-per-rev radial and axial vibrations. Lees [21] recently analysed a four-bearing, rigidly coupled shaft system and compared the level of second-harmonic response produced due to nonlinear bearings with that resulting from lateral-torsional coupling. He concluded that while it was likely that bearing nonlinearity was the major source of second-harmonic vibration over a wide range of conditions there were circumstances where coupling between lateral and torsional motion emerged as a significant source.

In summary, from the literature to date almost all of the analyses performed have assumed the main source of excitation to be related to $2\times$ forcing components produced by the interaction of mass unbalance and rotor speed fluctuations emanating from the Hooke's-joint effect. Interestingly, the author was unable to find any publication validating the assumption of equivalency between a misaligned flexible-element coupling and a hooke's-joint coupling. It is clear that more effort is required to enable a better understanding of the fundamental misalignment-vibration mechanism(s). The purpose of this paper therefore is to clarify the role and relative importance of the main rotor system parameters in producing complex vibration signatures in the presence of misalignment. In particular, the influence of coupling-stiffness anisotropy, bearing nonlinearity, mass unbalance and static torque-transmission effects will be investigated. Since the from and magnitude of coupling excitation forces is governed largely by the type of coupling employed, then to aid in the transparency of this study a simple coupling model is employed whereby coupling kinematic influences, such as the Hooke's-Joint effect, are excluded. This approach enables effective assessment of the role of other potentially important sources of system non-harmonic response.

2. Rotordynamic model

The model presented here is an extension of that described in [20]. The 5 degree-of-freedom (DOF) system model is shown in Fig. 1 and consists of two rigid rotors connected by a flexible-element coupling. The drive rotor (rotor1) is mounted on rigid supports and has a rotational degree of freedom, ψ. The driven rotor (rotor2) is supported on bearings having anisotropic stiffness and damping properties. Bearing nonlinear stiffness effects are also accounted for. The motion of rotor2 is fully defined by the shaft rotation angle φ, angular displacements α and β, and axial motion at the coupling, z_l, all of which are referenced to the inertial x–y–z axes. The flexible coupling has a single point of articulation, shown as point C in Fig. 1, and is therefore rigid in a radial sense. Coupling angular, torsional and axial flexibility are assumed in addition to torsional and axial damping. The model also includes for coupling angular stiffness anisotropy.

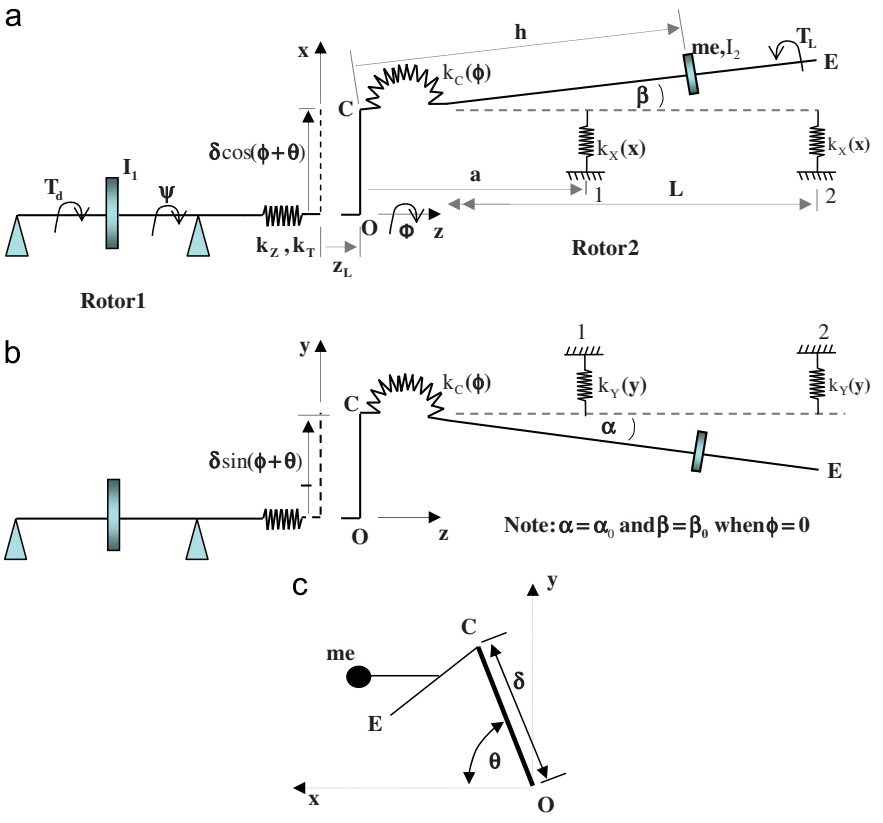

Fig. 1. Misalignment model: (a) z–x plane. (b) y–z plane. (c) x–y plane at t^*=0.

The orientation of the (uncoupled) misaligned shafts is determined by the parallel offset magnitude, δ and associated reference angle, θ in addition to the angular-offset angles α_0 and β_0. Drive torque, T_d, is assumed constant and applied at rotor1 while 'speed-squared' load torque is exerted at rotor2, thereby enabling investigation of torque transmission effects. Mass unbalance has been included in the driven rotor whose mass, m, is offset from the shaft geometric centre by an amount e. Coupling-hub skew, although included in the system model, is not considered in the current analysis as its influence is addressed fully in [20].

2.1. Shaft misalignment-pre-rotation considerations

It is first necessary to outline the assumptions made with regard to the relative positions of the drive and driven rotors in the uncoupled and coupled non-rotating states. For ease of visualisation the cases of angular and parallel misalignment are treated separately (Fig. 2), even though the approach is equally valid for combined misalignment. Fig. 2a shows the arrangement when only angular misalignment is present. The driven shaft is misaligned with respect to the drive shaft by an amount α_0 and β_0 about the x and y axes, respectively. The bearings and coupling element are unstressed at this point.

Subsequent coupling of the shafts will, in general, lead to the driven shaft taking up a new static position defined by the rotations α and β as shown in Fig. 2b. The coupling element and rotor bearings will now be subjected to a static preload. In contrast, when parallel misalignment, δ, is present it is assumed that coupling of the shafts does not immediately lead to a change in the strain energy of the coupling or bearings (Figs. 2c and d). Of course, subsequent shaft rotation will, in general, further alter this situation. The corresponding shaft displacements at the bearing locations are of great practical importance and the governing relationships are defined by Eq. (A.2) in Appendix A. However, in order to fully utilise this information it will be necessary first to obtain the system equations of motion.

2.2. Derivation of equations of motion—linear system

To obtain the equations of motion for the coupled system it is first necessary to derive the system kinetic and potential energy functions.

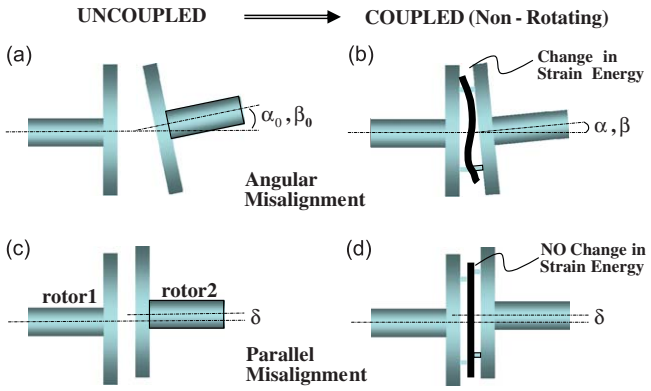

Fig. 2. Shaft misaligned static positions before and after coupling.

2.2.1. Energy expressions

The system generalized coordinate is described by

$$\{q\} = [\alpha, \beta, \psi, \phi, z_l] \tag{1}$$

The total kinetic energy, T, can be written in terms of the system translational and rotational velocities, so that $T = T_{\text{Trans}} + T_{\text{Rot}}$ where, referring to Eq. (A.3) in Appendix A the mass translational kinetic energy can be written as,

$$T_{\text{Trans}} = \tfrac{1}{2} m \cdot [\dot{x}_m^2 + \dot{y}_m^2 + \dot{z}_m^2] \tag{2}$$

and it can be shown that the combined rotational kinetic energy for rotors 1 and 2 is

$$T_{\text{Rot}} = \tfrac{1}{2} I_z[\omega_z^2] + \tfrac{1}{2} I_{x'}[\omega_{x'}^2] + \tfrac{1}{2} I_{y'}[\omega_{y'}^2] + \tfrac{1}{2} I_{z'}[\omega_{z'}^2] \tag{3}$$

where ω_x, ω_y and ω_z are the rotor1 angular velocities about the inertial axes while $\omega_{x'}$, $\omega_{y'}$ and $\omega_{z'}$ are the corresponding rotor2 body-axes angular velocities so that,

$$\omega_z = \dot{\psi}; \omega_{x'} = \dot{\alpha}\cos\beta - \dot{\phi}\sin\beta; \omega_{y'} = \dot{\beta}\cos\alpha + \dot{\phi}\sin\alpha; \omega_{z'} = \dot{\phi}\cos\alpha\cos\beta \tag{4}$$

Ignoring gyroscopic and rotary-inertia terms ($I_z = I_1$ and $I_{z'} = I_2$) the total kinetic energy can be written as

$$T = \left\{ \frac{1}{2} m \left[\begin{array}{l} [-e\dot{\varphi}\sin\varphi + \dot{\beta}h - \delta\dot{\varphi}\sin(\varphi+\theta)]^2 + [e\dot{\varphi}\cos\varphi + \delta\dot{\varphi}\cos(\varphi+\theta) - \dot{\alpha}h]^2 \\ +[e\cos\varphi(\dot{\varphi}\sin\alpha - \dot{\beta}) + e\sin\varphi(\dot{\alpha} + \dot{\varphi}\sin\beta) + \dot{z}_l - h\dot{\beta}\cos\alpha\sin\beta - h\dot{\alpha}\sin\alpha\cos\beta]^2 \end{array} \right] \right\}_{T_{\text{Trans}}}$$
$$+ \left\{ \frac{1}{2} I_1 \dot{\psi}^2 + \frac{1}{2} I_2 (\dot{\varphi}\cos\alpha\cos\beta)^2 \right\}_{T_{\text{Rot}}} \tag{5}$$

The system total potential energy, V, is derived from bearing and coupling strain energy in addition to gravitational effects,

$$V = V_{\text{brgx}} + V_{\text{brgy}} + V_{\text{cAng}} + V_{\text{cTors}} + V_{\text{cAxial}} + V_{\text{grav}} \tag{6}$$

which becomes,

$$\begin{aligned} V = {} & [\tfrac{1}{2} k_x \{[a(\beta - \beta_0) + \delta(\cos(\phi+\theta) - \cos\theta)]^2 + [L(\beta - \beta_0) + \delta(\cos(\phi+\theta) - \cos\theta)]^2\}]_{\text{brgx}} \\ & + [\tfrac{1}{2} k_y \{[a(\alpha_0 - \alpha) + \delta(\sin(\phi+\theta) - \sin\theta)]^2 + [L(\alpha_0 - \alpha) + \delta(\sin(\phi+\theta) - \sin\theta)]^2\}]_{\text{brgy}} \\ & + [\tfrac{1}{2} k_c \{(\alpha - \tau\cos\phi)^2 + (\beta + \tau\sin\phi)^2\}]_{\text{cAng}} \\ & + [\tfrac{1}{2} k_t \{\psi - \phi\cos\alpha\cos\beta\}^2]_{\text{cTors}} + [\tfrac{1}{2} k_z z_l^2]_{\text{cAxial}} - [m \cdot g \cdot [\alpha \cdot h + \delta\sin(\phi+\theta)]]_{\text{grav}} \end{aligned} \tag{7}$$

2.2.2. Coupling angular stiffness anisotropy

In the general case the coupling is assumed to exhibit angular stiffness anisotropy so that coupling angular stiffness about the stationery x and y axes, respectively, can be defined,

$$k_{c\alpha} = k_{co}[1 + \sum_{i=1}^{i=N} a_i \cos(i\phi + \lambda_i)] \text{and} k_{c\beta} = k_{co}[1 + \sum_{i=1}^{i=N} a_i \sin(i\phi + \lambda_i)] \tag{8}$$

The dimensionless coefficients a_i define the relative magnitudes of the coupling stiffness asymmetry components with respect to the coupling mean stiffness k_{co} and i=1, 2,…,N where N is the number of cyclic components required to define the coupling stiffness anisotropy. Note that while the coupling stiffness coefficients defined by (8) are clearly speed-dependent they remain independent of the system response and are therefore linear.

2.2.3. Generalised forces

2.2.3.1. Bearing damping forces. Non-conservative bearing viscous damping is introduced in the form of generalized forces, Q_{Di}, by considering the associated incremental work done δW. For our case, ignoring second- and higher-order terms and assuming small angles ($\sin x \approx x$; $\cos x \approx 1$), the generalized damping force vector is

$$\{Q_{Di}\}^{T} = \left\{ -C_y(a^2+L^2)\cdot\dot{\alpha} \;\vdots\; -C_x(a^2+L^2)\cdot\dot{\beta} \;\vdots\; -C_t\cdot\dot{\psi}+C_t\cdot\dot{\phi} \;\vdots\; -C_t\cdot\dot{\psi}-C_t\cdot\dot{\phi} \;\vdots\; -C_Z\cdot\dot{z}_l \right\} \tag{9}$$

2.2.3.2. External applied forces. The applied drive and load torques, T_d and T_L, are also generalized forces which, when transformed to the model stationary x–y–z coordinate system, give the corresponding generalized force vectors

$$\{Q_{Tdi}\}^{T} = \{ 0 \;\vdots\; 0 \;\vdots\; T_d \;\vdots\; 0 \;\vdots\; 0 \} \tag{10}$$

$$\{Q_{TLi}\}^{T} = \left\{ -\beta\cdot T_L \;\vdots\; \alpha\cdot T_L \;\vdots\; 0 \;\vdots\; T_L\cdot\cos\alpha\cdot\cos\beta \;\vdots\; 0 \right\} \tag{11}$$

For the purpose of subsequent analysis, drive torque T_d is considered constant and load torque T_L is assumed proportional to the square of the driven rotor speed ($T_L = c\cdot\dot{\phi}^2$).

2.2.4. Equations of motion

From Lagrange's Equations, where L is the Lagrangian (L=T−V), we get

$$\frac{d}{dt}\frac{\partial L}{\partial \dot{q}_i} - \frac{\partial L}{\partial q_i} = Q_i = Q_{Di} + Q_{Tdi} + Q_{TLi} \tag{12}$$

where Q_i contains all system generalized forces. The resulting system equations of motion can be written as

$$[M]\{\ddot{q}\} + [C]\{\dot{q}\} + [K]\{q\} = \{F\} \tag{13}$$

and these equations can be non-dimensionalised to give

$$[M^*]\{\ddot{q}^*\} + [C^*]\{\dot{q}^*\} + [K^*]\{q^*\} = \{F^*\} \tag{14}$$

Appendix B provides full details of the dimensional equations of motion, Eq. (13), and their dimensionless counterparts, Eq. (14).

2.3. Inclusion of nonlinear bearings

Nonlinear bearing stiffness forces are obtained by applying Newton's method. These forces are then added to the earlier derived linear bearing forces to simulate bearings exhibiting 'hardening-spring' characteristics (Fig. 3). The additional bearing stiffness force resulting from nonlinear influences is assumed to take the general form,

$$F_{knl} = k_n\cdot \mathrm{sign}(x)\cdot |x|^m \tag{15}$$

The parameters k_n and m determine the magnitude and nature of the bearing nonlinear stiffness. The nonlinear bearing forces produce bending moments, $M^*_{N\alpha}$, $M^*_{N\beta}$ and $M^*_{N\phi}$, about the x, y and z axes, respectively as shown in Appendix C. The resulting dimensionless moments $M^*_{N\alpha}$, $M^*_{N\beta}$ and $M^*_{N\phi}$ are presented in Eqs. (C.8)–(C.10), Appendix C.

To enable the inclusion of bearing nonlinear stiffness effects in the equations of motion, Eq. (14) is updated so that force vector $\{F^*\}$ is replaced with modified force vector $\{F^*\}_{NL}$, to give the final dimensionless equations of motion,

$$[M^*]\{\ddot{q}^*\} + [C^*]\{\dot{q}^*\} + [K^*]\{q^*\} = \{F^*\}_{NL} \tag{16}$$

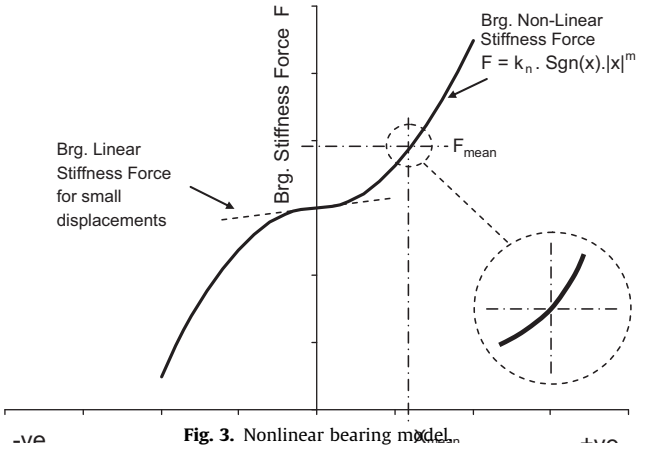

Fig. 3. Nonlinear bearing model.

where

$$\{F^*\}_{NL} = \{F^*\} + \left\{ M^*_{N\alpha} \quad \vdots \quad M^*_{N\beta} \quad \vdots \quad 0 \quad \vdots \quad M^*_{N\phi} \quad \vdots \quad 0 \right\}^{\mathrm{T}} \tag{17}$$

3. Analysis

3.1. Analysis approach and model parameters

The system equations of motion (17) were solved numerically using Matlab routine ode45 to compute the transient response for a variety of model configurations designed to enable assessment of a number of important system parameters in isolation. In each case the analysis was run until a steady-state solution was reached and FFT applied to the subsequent time-record to obtain amplitude–frequency information. The dimensionless time-step, $\Delta t*$ was set at 0.03. In all analyses cases rotor2 overhang dimension a^* is set at 0.1 and its mass m is considered located centrally between the bearings, i.e. h^*=0.55. Additionally, it is assumed that rotor2 inertia is small in comparison with that of rotor1, so that $r1/r2$=10 and $r1$=1.0. For data presentation purposes shaft displacements and bearing forces are shown only for bearing 2 location, denoted as point E in Fig. 1.

3.2. Static displacements and forces (non-rotating system)—misalignment only

Table 1 provides a summary of the model dimensionless parameters selected for the static (non-rotating) analyses presented here. Where alternative parameter values have been used this has been highlighted.

The system static displacements and forces are easily obtained from Eq. (13) by eliminating all dynamic variables [20]. For presentation purposes the shaft angular displacements are normalized with respect to the original misalignment, α_0 and the bearing forces are normalized with respect to the bearing force which would occur if the shaft displacement was set equal to the respective misalignment value (i.e. α_0 for angular and p for parallel misalignment). Linear bearings are assumed for the static cases to enable transparency in the result interpretation.

3.2.1. Angular misalignment only ($\alpha_0 \neq 0$; β_0=0)

Figs. 4a and b illustrate the influence of coupling stiffness and transmitted torque on the driven shaft static displacement and bearing loading, respectively, when subjected to angular misalignment. Both figures confirm that when the shafts are coupled, with no torque present, then system static displacements and bearing preloads are induced, in the plane of the original misalignment (i.e. β=0). Shaft displacements and bearing loading increase as coupling stiffness is increased. This effect is amplified as torque is applied, since the increased tendency of the driven shaft is to align itself with the drive shaft. It is seen that the application of torque in the presence of angular misalignment leads to the emergence of shaft static deflections and bearing loading normal to the misalignment plane. The plots also show there is an intermediate torque level at which these normal displacements and bearing forces reach a maximum value.

When bearing stiffness anisotropy ($k_1 \neq 1$) is introduced, although not shown here, a reduction in the shaft displacement in the direction of increased bearing stiffness is observed in addition to the increased bearing force in this direction.

3.2.2. Parallel misalignment only ($p \neq 0$; θ=90°)

Initially the rotational axes of both shafts are parallel and offset, by the dimensionless amount p, in the y–z plane. The shafts remain in this position even when coupled and the bearings remain unloaded. However, upon slow rotation

Table 1
Model default parameter values—static case.

Parameter description	Symbol	Value
Coupling angular stiffness	k^*_{co}	Variable
Steady-state rotor speed	$\dot{\phi}^*$	0
Drive torque	T^*_d	Variable
Brg. linear-stiffness anisotropy	k_1	1 or 3
Brg. nonlinear stiffness constants	k_{nx}, k_{ny}	0
Cplg. anisotropy parameter	k_v	0
Angular misalignment	α_0	$\neq 0$
Angular misalignment	β_0	0
Parallel offset	p	0.002
Parallel offset reference angle	θ	90°
Gravity constant	g^*	0

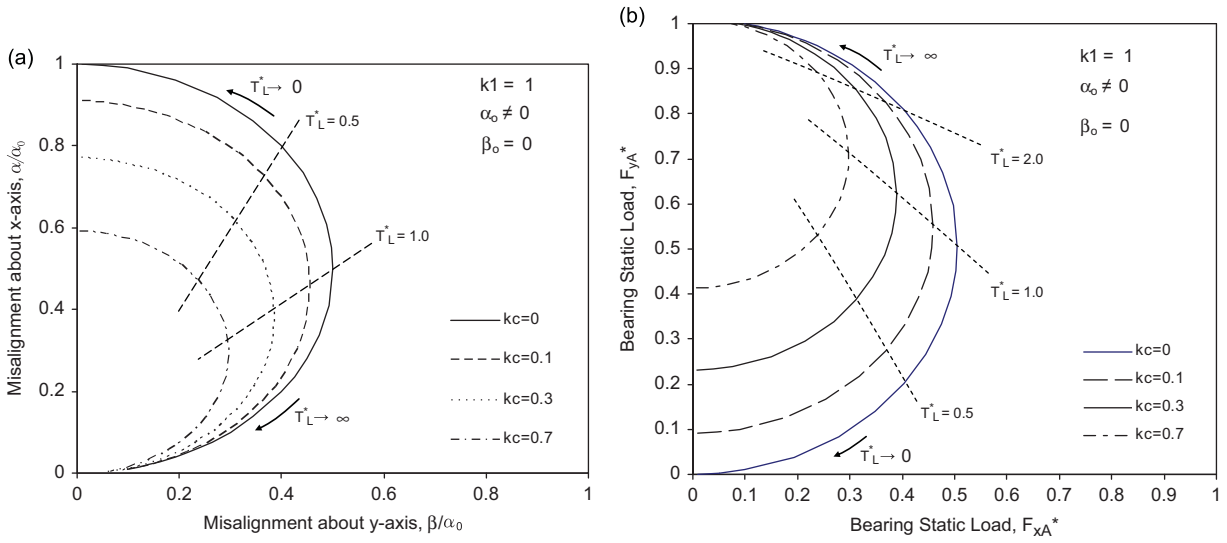

Fig. 4. Angular misalignment: (a) Shaft static displacement. (b) Static bearing loads.

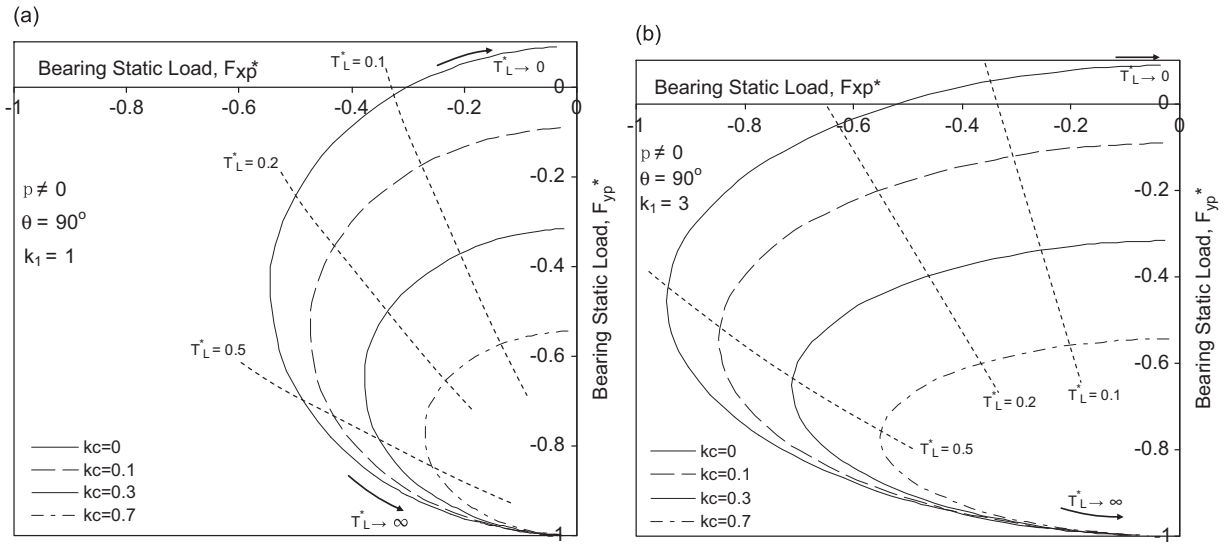

Fig. 5. Parallel misalignment – static bearing loads: (a) k_1=1. (b) k_1=3.

of the shaft system the driven shaft is displaced from its original position and both shafts are subjected to fluctuating forces. Fig. 5a plots the locus of the mean value of the force (preload) induced at bearing 2 as a function of coupling stiffness and transmitted torque, for the isotropic bearing arrangement. As with the case of angular misalignment, increasing the coupling angular stiffness leads to larger bearing static forces in the misalignment plane.

Additionally, the introduction of torque amplifies the bearing forces while inducing bearing loads normal to the plane of the misalignment. Shaft static displacements, although not shown, follow the same pattern as the presented bearing forces. The maximum displacements (and bearing loads) occur when the coupling becomes rigid and/or when the transmitted torque is large. The bearing stiffness anisotropy (k_1=3) leads to reduced shaft displacements in the direction of increased bearing stiffness and corresponding increased bearing static loading (Fig. 5b).

It is clear from the preceding sections and reference to Figs. 4 and 5 that the relative orientation of angular and parallel misalignment would have a considerable influence on the resultant magnitude and direction of the induced bearing forces. This is important, particularly in machinery utilizing fluid-film bearings whose properties can vary greatly depending on the magnitude and direction of the bearing static loading.

3.3. Dynamic response—rotating system

Table 2 provides a summary of the model nominal dimensionless parameters selected for the dynamic (i.e. rotating) analyses presented here. Where alternative parameter values have been employed they are clearly highlighted in the relevant section.

For these simulations nonlinear bearings are assumed (k_{nx} & $k_{ny}\neq 0$). The dynamic analyses were performed using a 'low' drive torque setting just sufficient to balance the load torque and ensure a stable operating speed, therefore the influence of drive torque on the system dynamic response can be considered negligible. In addition, analysis results are presented mainly for shaft motions in the x-direction, x_2^*, as the response normal to this was found to be largely unaffected by the misalignment effect.

3.3.1. Angular misalignment only (β_0=0.002)

Examination of Eq. (14) shows that when shaft rotation is introduced in the presence of angular misalignment the system static displacements and forces remain unchanged and there is no dynamic response [20]. However, an induced internal static loading (i.e. preload) does lead to each rotating element being subjected to stress reversal as demonstrated in the following section.

3.3.1.1. Angular misalignment with mechanical unbalance (β_0=0.002; u=0.001). The misalignment-induced static preload leads to a change in the static bearing stiffness so that when mass unbalance is introduced the driven shaft will vibrate along a different portion of the nonlinear stiffness characteristic curve (Fig. 3). Fig. 6a shows the resulting non-circular shaft displacement orbits which exhibit asymmetry about the y-axis due to the preload being applied along the x-axis. Increasing the coupling stiffness also augments the bearing static preload (Fig. 6b) leading to reduced 1-per-rev bearing-force response while introducing a small but significant second-harmonic component. The coupling transmitted force consists of combined static and dynamic components (Fig. 6c) both of which increase as the coupling stiffness is raised. Increased coupling stiffness may exist, for example, in cases of severe misalignment where the coupling is forced to operate in its nonlinear region. The coupling static force results directly from the mechanical unbalance force and its magnitude is determined by the relative angular location of the mass unbalance and the respective element fixed on the coupling. In the case shown in Fig. 6c the transmitted force is computed for a coupling element considered to be in-line with the unbalance (i.e. θ=0°). The coupling elements are seen to be subjected to a predominantly synchronous alternating force which emanates from the imposition of the misalignment-induced static preload. This raises the prospect of fatigue failure in the rotating components.

3.3.1.2. Angular misalignment with coupling stiffness anisotropy (β_0=0.002; k_v=0.2). The analyses presented within are performed for a specific coupling stiffness characteristic which is representative of a commonly employed disc-type, flexible-element coupling discussed in [4,10]. Coupling angular stiffness, about the x and y axes, respectively, is defined by,

$$k_{c\alpha} = k_c\{1 - k_v[1 - |\cos(n_p \cdot \phi + \lambda + (\pi/2))|]\} \tag{18}$$

Table 2
Model default parameter values—dynamic case.

Parameter description	Symbol	Value
Coupling angular stiffness	k_{co}^*	0.05
Steady-state rotor speed	$\dot{\phi}^*$	0.75
Drive torque	T_d^*	8.e−5
Brg. linear-stiffness anisotropy	k_1	1.0
Brg. nonlinear stiffness constants	k_{nx}, k_{ny}	110
Brg. nonlinear stiffness force exponents	m_x, m_y	2
Cplg. anisotropy parameter	k_v	0.2
Cplg. anisotropy order	n_p	1
Angular misalignment	α_0	0
Angular misalignment	β_0	0.002
Parallel offset	p	0.002
Parallel offset reference angle	θ	0°
Gravity constant	g^*	0
Mass-eccentricity	u	0.001
Torsional frequency ratio	f_t	1.3
Axial frequency ratio	f_z	0.1
Bearing damping factor—x direction	ζ_x	0.03
Bearing damping factor—y direction	ζ_y	0.03
Coupling axial damping factor	ζ_z	0.01
Coupling torsional damping factor	ζ_t	0.001
Cplg. hub skew	τ	0

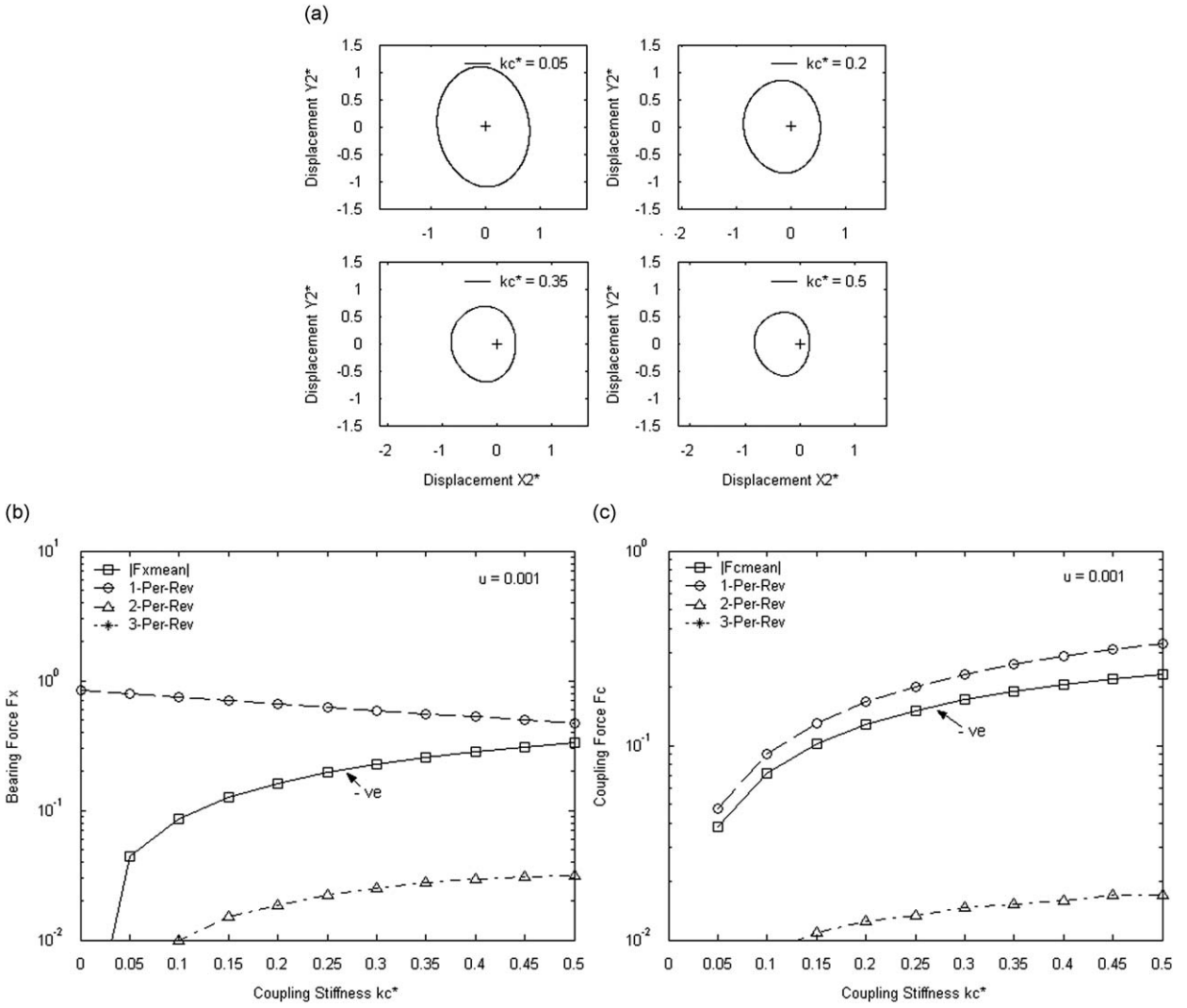

Fig. 6. Combined angular misalignment and mass unbalance: (a) Shaft displacement. (b) Bearing 2 transmitted force. (c) Coupling transmitted force.

and

$$k_{c\beta} = k_c \cdot \{1 - k_v \cdot [1 - |\cos(n_p.\phi + \lambda)|]\} \tag{19}$$

where k_v represents the ratio of coupling stiffness variation to the maximum coupling stiffness and n_p is the number of coupling bolt-pairs or alternatively the number of 'defects', where a defect may be considered as a localized reduction in coupling stiffness. The stiffness coefficients are clearly linear and speed-dependent. Fig. 7 shows the characteristic stiffness function ($k_{c\alpha}$ versus ϕ) for a coupling considered to have a single defect (n_p=1), which produces a 2-per-rev stiffness variation. The angular location of the defect is referenced to a plane fixed on the driven rotor and coincidental with the misalignment-plane at zero rotation ($\dot{\phi}^* = 0$), using the angle λ. For the cases considered in this section λ=0°.

Fig. 8a shows that the static preload resulting from angular misalignment interacts with the coupling anisotropy leading to a dominant 2-per-rev shaft response along the x-axis. The plot is for a fixed rotor speed $\dot{\phi}^* = 0.75$ and the resulting shaft response is seen to be further amplified as coupling stiffness is increased. There is no vibration response normal to the preload direction so that the shaft motion is along a line coincident with the x-axis. Although the response levels are relatively low there are other factors that can make the anisotropy effect more pronounced. Fig. 8b illustrates how the coupling anisotropy excites the system natural frequency at speeds corresponding to $\frac{1}{4}$ and $\frac{1}{2}$ of the natural frequency, as a result of the 4-per-rev and 2-per-rev excitations, respectively. In addition, the relative importance of this effect in real machinery would clearly be greatly dependent upon the level of damping present, an important factor in machinery having low damping, such as rolling-element bearing installations.

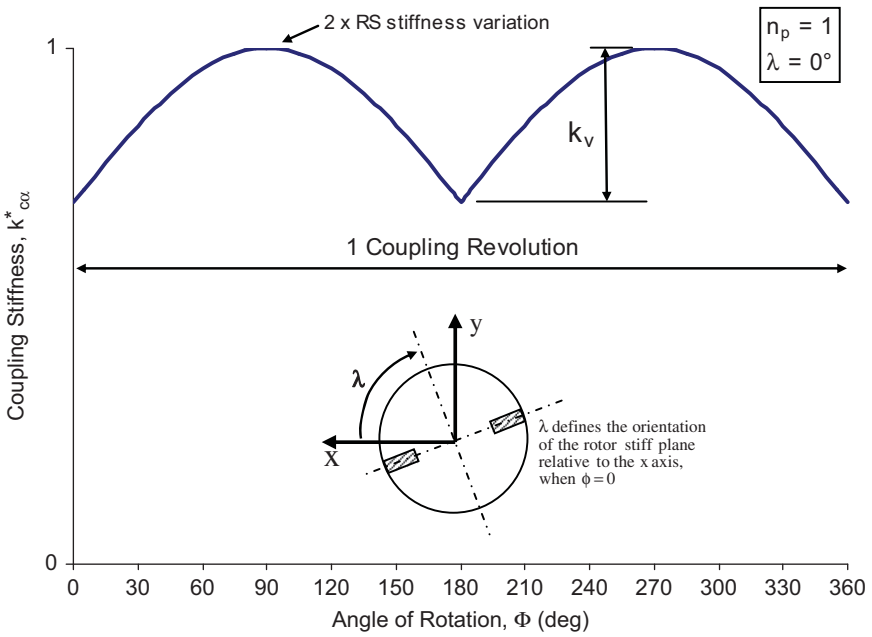

Fig. 7. Coupling anisotropic stiffness characteristic.

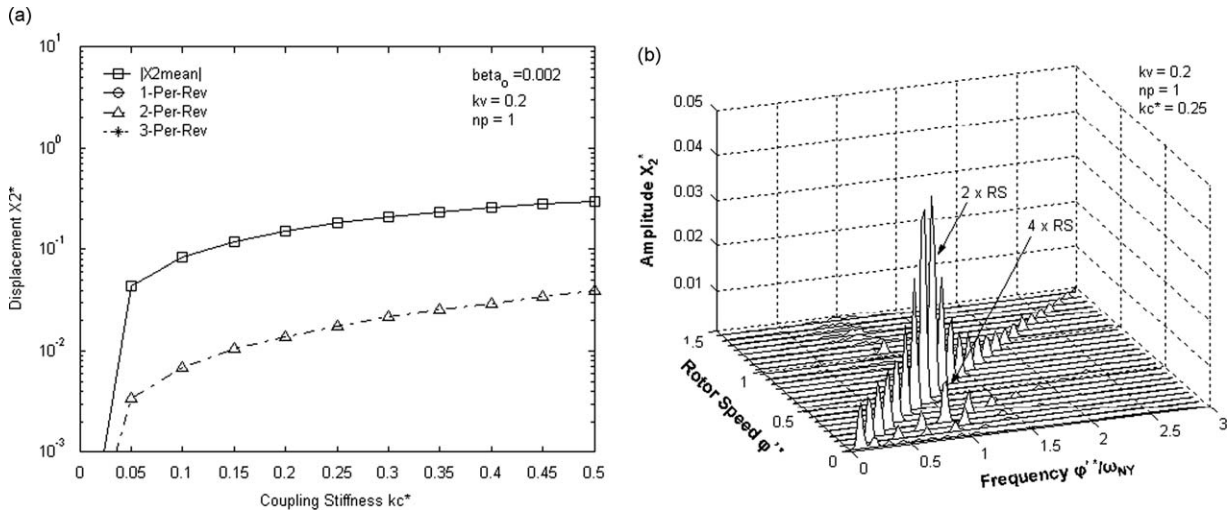

Fig. 8. Combined angular misalignment and coupling stiffness anisotropy: (a) Shaft displacement versus coupling stiffness. (b) Shaft displacement cascade plot.

3.3.2. *Parallel misalignment only (p=0.002; θ=0°)*

The model results show that, in contrast to angular misalignment, parallel misalignment produces both static *and* dynamic system response. The parallel offset, *p*, creates a crank-effect where the crank-arm is denoted by the line OC in Fig. 1c. The shaft coupling end, shown as point C, is subjected to synchronous displacement excitation. The driven shaft response, although dominated by a synchronous component, in general contains higher harmonics (Fig. 9a). It is seen that as the coupling stiffness k^*_{co} is increased the shaft mean position, in the direction of the *x*-axis, is displaced further from its original position. The shaft mean position along the *y*-axis remains unaltered. In conjunction with this, the shaft displacement orbits become more distorted as second-harmonic content is raised (Fig. 9b). Increasing the offset *p* also increases the bearing preload resulting in greater bearing stiffness asymmetry and therefore has a similar effect. In particular, increased misalignment produces multi-harmonic shaft speed fluctuations (Fig. 9c). Such speed fluctuations could be important in exciting system torsional frequencies in some circumstances [20].

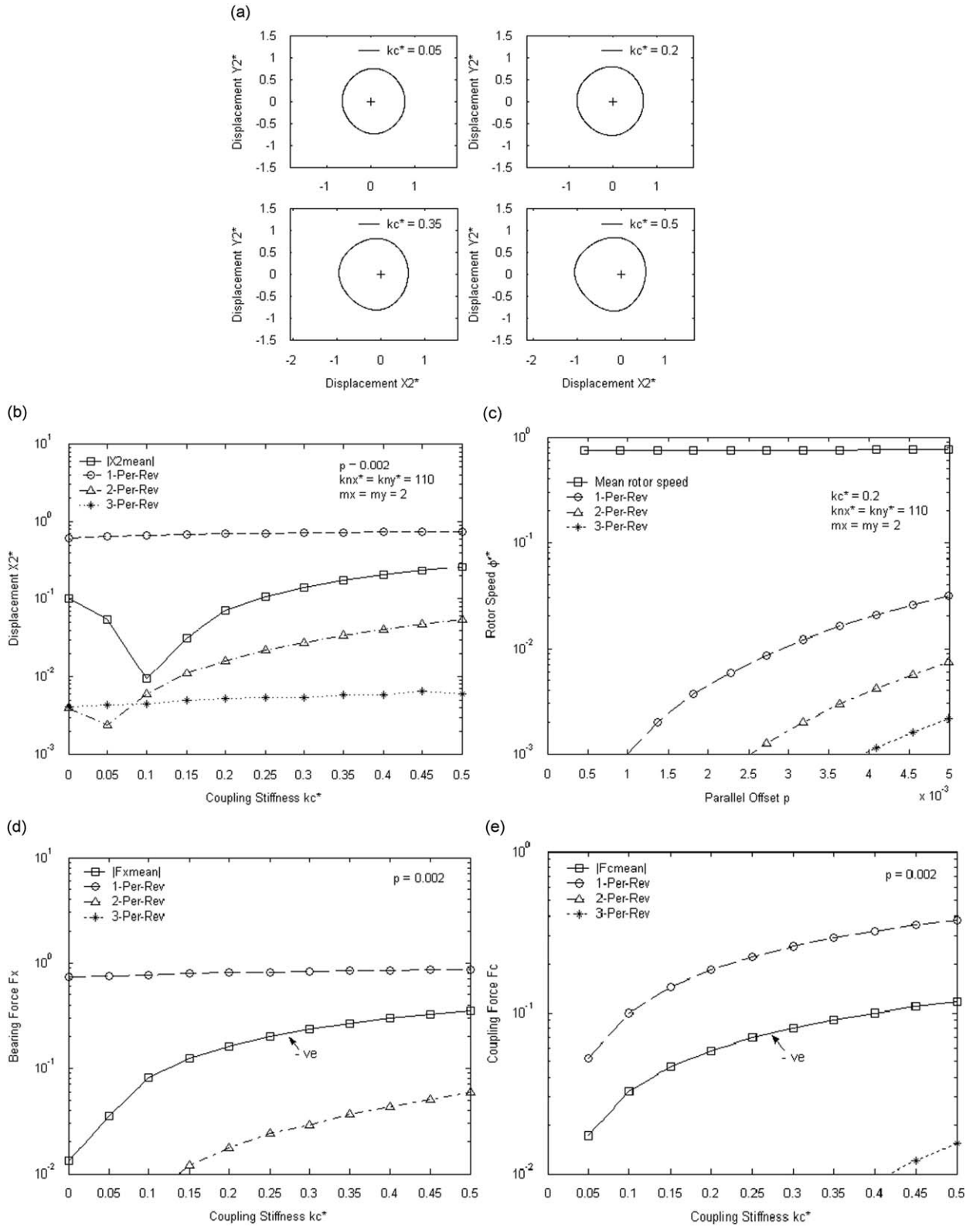

Fig. 9. Parallel misalignment only: (a) Shaft response orbits. (b) Shaft displacement x_2^*. (c) Rotor speed versus offset p. (d) Bearing Force F_x (e) Coupling transmitted force F_c.

Bearing forces follow the pattern of shaft displacements. In the plane of the misalignment static, first and second-harmonic bearing-force components are present and increase with coupling stiffness (Fig. 9d). The coupling transmitted force is dominated by 1-per-rev fluctuation (Fig. 9e), resulting from the misalignment-induced static preload, which imposes stress-reversal on the coupling flexural elements. As shown, a significant static coupling force also exists.

3.3.2.1. Parallel misalignment with mechanical unbalance (p=0.002; u=0.001). As expected, the addition of mass unbalance has a substantial influence on the shaft and bearing-force response. Shaft displacement is predominantly synchronous but significant second- and third-harmonic components are also influenced by the unbalance (Fig. 10a), due to bearing nonlinearity. The resultant system response is mainly governed by the angle θ which fixes the misalignment plane in the stationary axes and also determines the relative angular orientation of the unbalance with respect to the misalignment 'crank-arm' OC (Fig. 1c). The shaft static displacement of course remains unaltered and is therefore not shown. Fig. 10a shows that, for a fixed speed of $\dot{\phi}^* = 0.75$, the first three harmonic components of displacement can be minimized when $\theta \approx 160^\circ$. This 'optimum' value of θ will vary depending on the operating speed, $\dot{\phi}^*$ and misalignment offset value, p. This is because the dynamic behaviour of a system with parallel misalignment and unbalance is very similar to one where mass unbalance is combined with a shaft bow. Therefore, the model results indicate that vibration resulting from misalignment could be substantially reduced through mechanical balancing, though selection of the correction mass and angular location using conventional balance procedures may be more difficult due to the presence of system nonlinearities. Of course, even if dynamic response is reduced using this approach the static bearing preload would still remain.

Another interesting aspect is the influence of the unbalance angular location on the magnitude of the 1-per-rev speed fluctuation (Fig. 10b). The speed fluctuation is greatest when θ=90° and 270°, i.e. when the unbalance is normal to the 'crank-arm'. This effect is thought to be related to the unbalance-mass tangential acceleration forces whose magnitude would vary according to the angular location of the unbalance.

3.3.2.2. Parallel misalignment with coupling stiffness anisotropy (p=0.002; θ=0; k_v=0.2). Coupling stiffness anisotropy was simulated by applying the stiffness characteristics defined by Eqs. (18) and (19) for a shaft speed of $\dot{\phi}^* = 0.75$. The parameter λ specifies the angular location of the stiffness 'defect' in relation to the misalignment crank-arm OC (Fig. 1c). Fig. 11a shows the computed shaft displacement x_2^* as a function of the coupling stiffness, k_c^*, for λ=0° and k_v=0.2. Although the displacement trends are seen to be similar to those for the case of parallel misalignment alone (Fig. 9b) the inclusion of coupling anisotropy has significantly reduced the second-harmonic component while only slightly altering the static displacement. The full influence of the anisotropy becomes clearer in Fig. 11b where the importance of the angular location of the stiffness defect is evident. The misalignment-induced static preload interacts more effectively with the anisotropy when the stiffness defect is normal to the misalignment crank-arm (λ=90° or 270°) to produce a substantial increase in the 2-per-rev vibration. However the maximum amplitudes are relatively low representing approximately 3 percent of the first-harmonic and 30 percent of the mean displacement values, respectively. The mean shaft displacement is also seen to be sensitive to the location of the anisotropy, exhibiting a variation of more than 30 percent.

Fig. 11c confirms that, for this case, even when the coupling anisotropy is substantial (k_v=0.5) the shaft motion is still dominated by synchronous response and the anisotropy associated component, i.e. the second-harmonic, is small by comparison. Clearly this situation can change depending upon the proximity of the anisotropy-related excitation

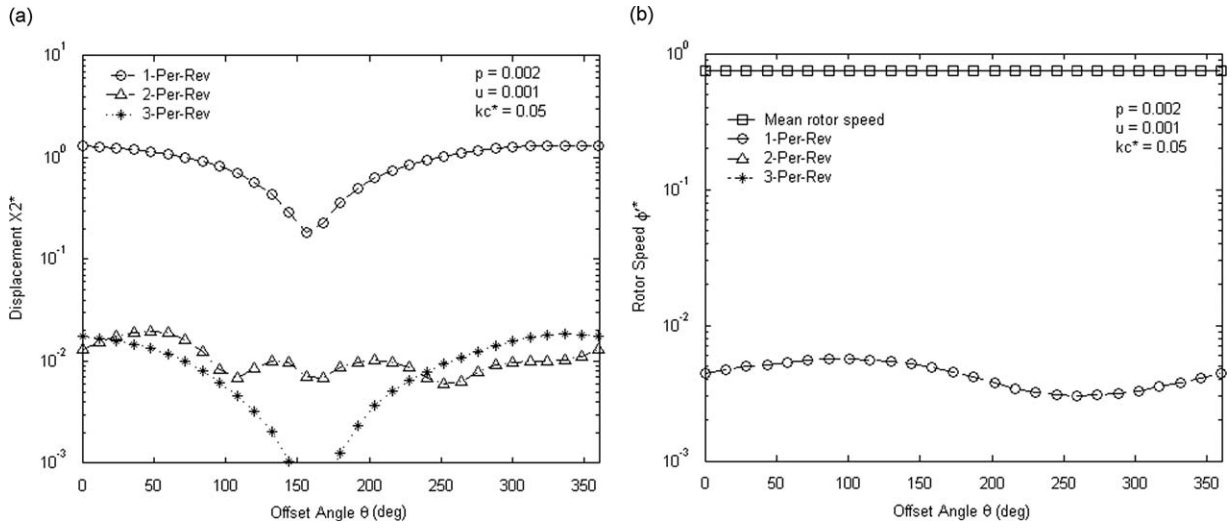

Fig. 10. Combined parallel misalignment and mechanical unbalance: (a) Shaft displacement versus offset angle θ. (b) Rotor speed versus offset angle θ.

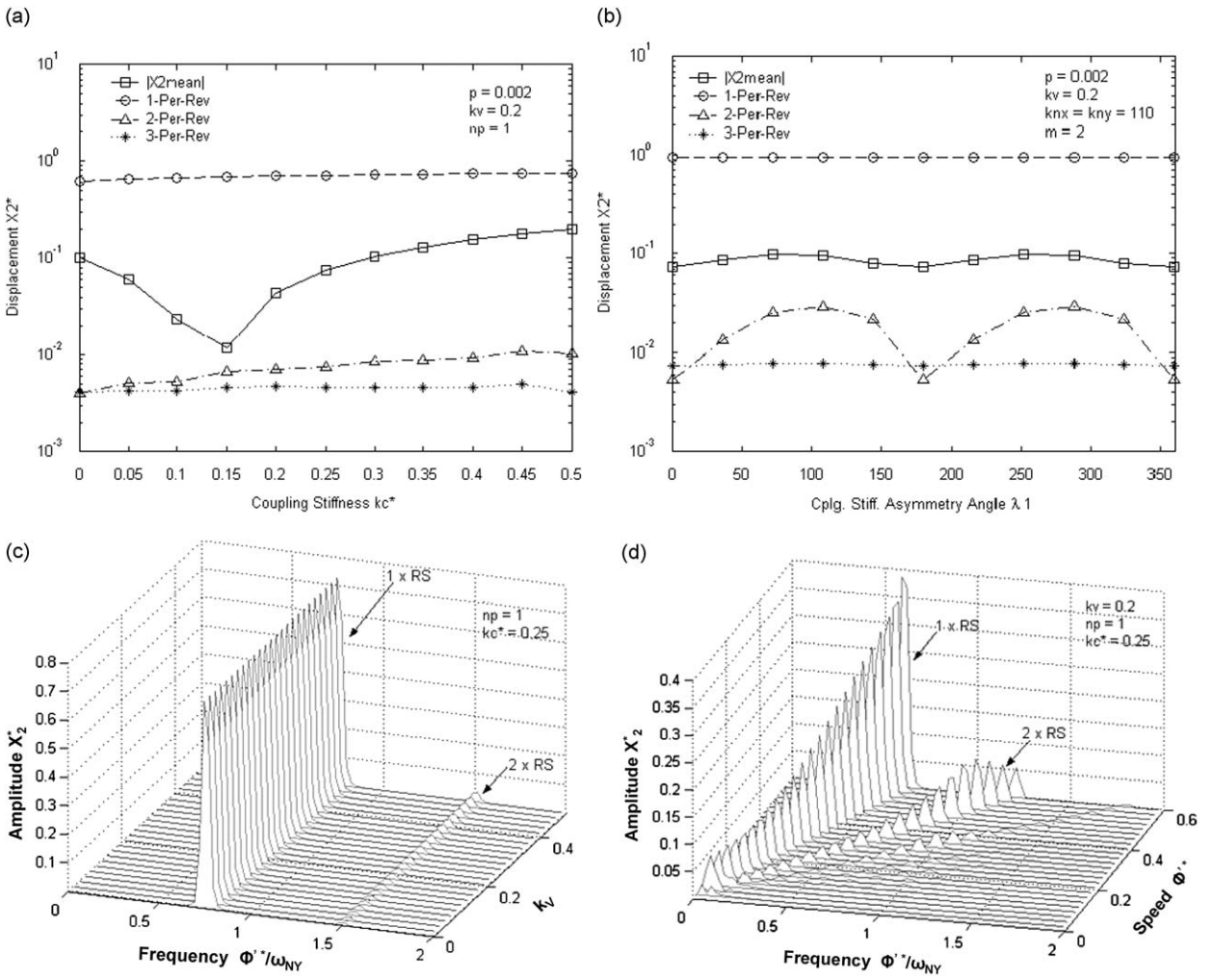

Fig. 11. Combined parallel misalignment and coupling anisotropy: (a) Shaft displacement versus coupling stiffness. (b) Influence of anisotropy orientation angle λ. (c) Influence of anisotropy parameter k_v. (d) Shaft displacement cascade plot.

frequencies and the system natural frequencies. This feature is demonstrated in Fig. 11d where the shaft displacement frequency spectrum is shown for a speed range $\dot{\phi}^* = 0$ to 0.6. As the rotor speed reaches a value corresponding to half of the first natural frequency the double-frequency vibration emerges strongly and is now a much larger proportion of the total response.

3.3.3. *Influence of increased bearing stiffness nonlinearity*

It is important to consider the influence of nonlinear effects which can play a major role in modern rotating machinery due to for example rolling-element [13] or fluid-film [14,21] bearings. In the earlier simulations a 'low-level' of bearing nonlinearity was assumed ($k^*_{nx,ny} = 110$; $m_{x,y} = 2$) to aid in focusing the analyses on the influence of other parameters unrelated to bearing nonlinearities. This nonlinear stiffness value was considered low since for shaft dimensionless displacements of approximately 0.001 the estimated change in system natural frequency was less than 1 percent. Consequently, in this section a greater range of nonlinear parameters is considered. Fig. 12a illustrates the influence of parallel misalignment on the model natural frequency for two different forms of bearing stiffness nonlinearity, i.e. for $m_{x,y}$=2 with $k^*_{nx,ny} = 0.4e3/1.0e3$ and $m_{x,y}$=3 with $k^*_{nx,ny} = 0.4e6/1.0e6$. The maximum values for the stiffness coefficients, $k^*_{nx,ny}$ (1.0*e*3 for $m_{x,y}$=2; 1.0*e*6 for $m_{x,y}$=3), were chosen so that, for a realistic dimensionless shaft deflection (x_2/L) of 0.001, the bearing force produced in the nonlinear systems would be twice that for the linear case. Therefore, for the purpose of this work these maximum nonlinear stiffness values are considered 'high' due to their significant influence in increasing the system natural frequency ($>5\%$) for moderate levels of displacement. Consequently, all other nonlinear stiffness values used in the analyses were selected relative to these values to simulate bearings having stiffness qualities covering a range

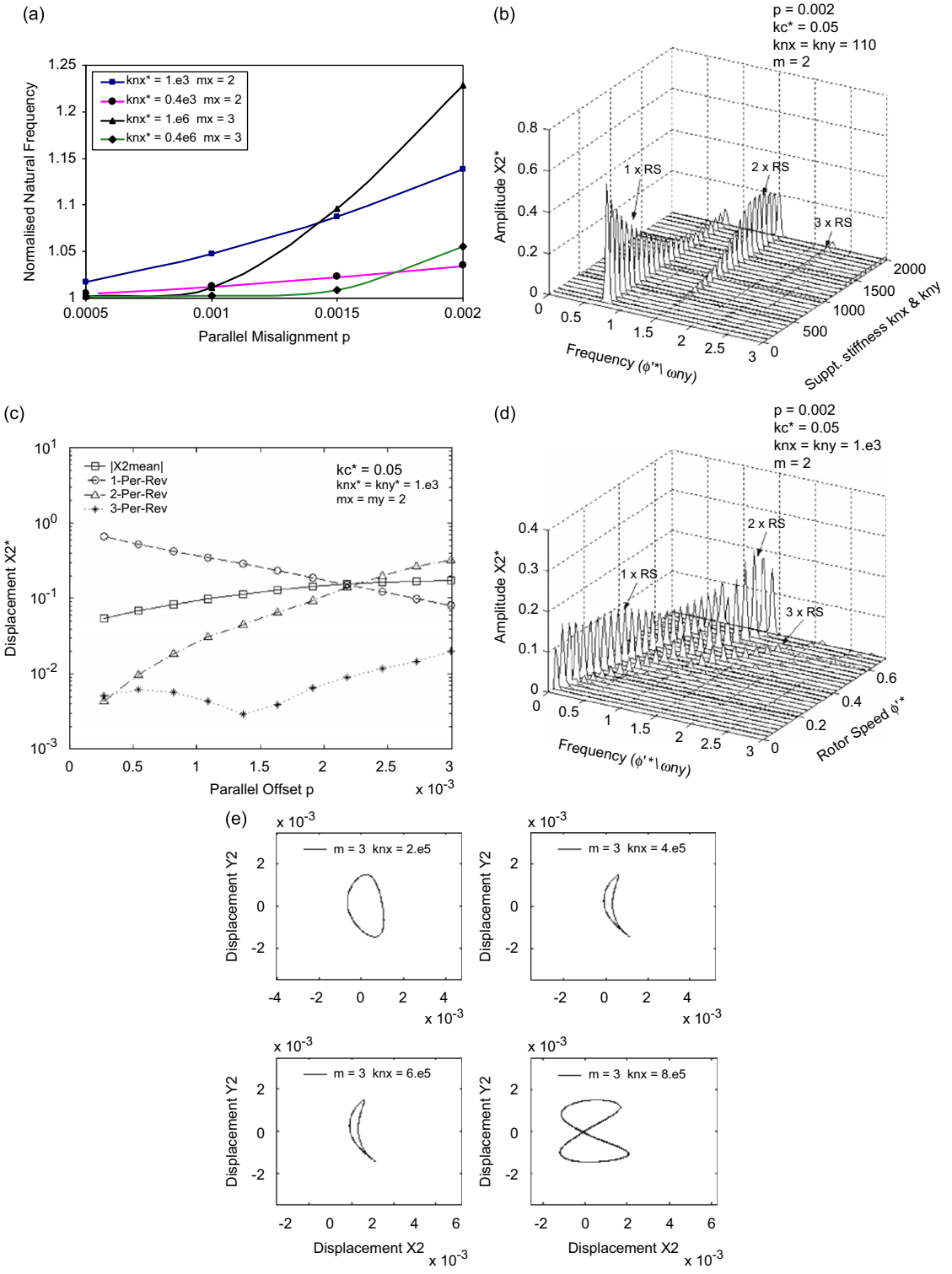

Fig. 12. Combined parallel misalignment and nonlinear bearings: (a) Natural frequency variation. (b) Shaft displacement spectral content. (c) Influence of parallel offset p. (d) Shaft displacement cascade plot. (e) Effect of increased bearing nonlinearity.

from linear to 'highly' nonlinear. The figure shows the influential effect of the misalignment offset, p, in raising the system natural frequency as a result of the increased static preload.

Figs. 12b–d, describe the model vibration response when the bearing nonlinear stiffness force exponents, m_x and m_y are set at 2. The effect of increasing nonlinear coefficients k^*_{nx} and k^*_{ny}, for fixed speed $\dot{\phi}^* = 0.75$, is clearly demonstrated in Fig. 12b. It is shown that only simple harmonic response is exhibited when linear bearings are employed, i.e. when $k^*_{nx} = k^*_{ny} = 0$. This is to be expected for a purely linear system subjected to harmonic excitation. However, as the bearing nonlinearity is enhanced this harmonic motion is transformed into multi-harmonic response, dominated by 2-per-rev vibration. The influence of increasing parallel offset, p on the shaft displacement response for a case considered to represent 'high' bearing nonlinearity ($k^*_{nx} = k^*_{ny} = 1.0e3$) is illustrated in Fig. 12c. The emergence of a strong 2-per-rev vibration component results from the increased static preload which increases the bearing nonlinearity as demonstrated in Fig. 3. Another important aspect in parallel misaligned nonlinear systems is the proximity of rotor speed harmonics to system natural frequencies. Fig. 12d shows how the shaft displacement harmonic content can vary significantly with rotor speed and system resonances can occur at speeds corresponding to submultiples of the rotor system natural frequencies. In this case clear resonances are observed at one-third and one-half of the rotor system first natural frequency.

The bearing nonlinear force-shaft displacement characteristic selected for the analysis will clearly play a major role in determining the form and magnitude of the system response. In Fig. 12e the shaft displacement trajectories are shown for the same constant speed case where increasing bearing nonlinearity is considered ($k^*_{nx} = k^*_{ny} = 0.2e6 - 0.8e6$) and quadratic bearing stiffness ($m_{x,y}$=3) is assumed. The shaft displacement plots presented are considered typical of those frequently observed in the field on rotating machinery having fluid-film bearings and subjected to misalignment, where significant second-harmonic response is characteristic. These plots provide further confirmation of the important role of parallel misalignment in conjunction with system nonlinearities in producing harmonically rich rotor system vibration signatures.

4. Conclusions

A representative shaft misalignment model which incorporates many of the important characteristics present in real rotating machinery has been presented. The model was used to study the dimensionless dynamic response of flexibly coupled misaligned rotors when subjected to parallel and angular misalignment. The influence of a number of key system parameters including bearing nonlinearity, coupling anisotropy, mass unbalance and drive torque was assessed.

This study shows that shaft displacements and bearing forces resulting from angular and parallel misalignment are fundamentally different. Both types of misalignment lead to the imposition of a static bearing preload. However, in the absence of other (internal or external) excitation sources, only parallel misalignment produces system dynamic response while angular misalignment generates purely static forces and displacements.

Parallel misalignment-induced dynamic excitation is predominantly synchronous in nature due to the parallel-offset crank-arm effect which also produces fluctuations in the rotor speed. In both misalignment cases the resulting static preload can play a major role in creating complex vibration response through interaction with rotating-element anisotropy and bearing nonlinearities. It is worth noting that in contrast to nonlinear bearing effects, coupling anisotropy generates response-harmonics due to the presence of speed-dependent, but linear, stiffness coefficients. Both coupling stiffness anisotropy and bearing nonlinearity lead to modification of the system response mainly in the plane of the misalignment. Also, the rotating elements are subjected to alternating forces which may raise fatigue issues. Increasing coupling stiffness results in the imposition of greater static bearing forces, static shaft displacements and rotating-element alternating forces. This effect is reinforced further by the application of low-level drive torque.

The model results showed that the introduction of rotating-element anisotropy and bearing nonlinearity in the presence of misalignment resulted in augmentation of complex multi-harmonic system response, with dominant vibration amplitudes observed to occur mainly at rotor speed and its second harmonic. In the misalignment cases studied the introduction of bearing nonlinearity had a more dramatic effect in altering the system vibration response than that of rotor anisotropy.

In all cases the coupling stiffness was found to be a major controlling factor in determining the system dynamic response. While increasing the coupling stiffness led to greater shaft vibration response and dynamic bearing forces in parallel-misaligned systems the opposite was found to be true for angularly misaligned systems.

In well-aligned rotor systems vibration response is governed mainly by the amount of mass unbalance, level of damping available and proximity of running-speed to system natural frequencies. However, the investigation performed here shows that in misaligned machinery a number of *additional* influential parameters can greatly alter the nature and level of rotor vibration, rotating-element stresses and associated bearing forces:

- Misalignment type (angular or parallel) and magnitude
- Coupling stiffness
- Relative orientation of mass unbalance
- Magnitude and relative orientation of rotating-element anisotropy
- Magnitude and form of bearing nonlinearities
- Proximity running-speed harmonics to system natural frequencies

- Relative orientation of angular and parallel misalignment
- Drive torque magnitude

The results presented here probably go some way to explain the main reasons for the observed variability in the vibration character of apparently similar, or even identical, misaligned machines.

More specifically, based on the work presented here and in [20,21] it is the author's contention that, even though numerous factors influence the misalignment-vibration relationship, one of the major contributory factors towards the production of 2-per-rev and other harmonic vibration components is most likely the modification of system properties resulting from interaction of the misalignment-induced static preload with machine component nonlinearities such as those present in fluid-film and rolling-element bearings.

To the author's knowledge the misalignment model presented within addresses many important features not previously studied in the technical literature.

Acknowledgement

The author acknowledges the support of Saudi Aramco, Saudi Arabia.

Appendix A

A.1. Coordinate transformation

Assuming the body axes for rotor2 to be x'–y'–z' then the location of any point on the driven shaft can be transformed to the inertial coordinate system x–y–z from, $\{X\} = [T] \cdot \{X'\} + \{X_0\}$ where $\{X\}^{\mathrm{T}} = \{x\ y\ z\}$, $\{X'\}^{\mathrm{T}} = \{x'\ y'\ z'\}$ and $\{X_0\}^{\mathrm{T}} = \{\delta \cdot \cos(\phi+\theta)\ \ \delta \cdot \sin(\phi+\theta)\ \ z_l\}$. T is the transformation matrix and for small angles, α and β, the relationship becomes

$$\begin{Bmatrix} x \\ y \\ z \end{Bmatrix} = \begin{bmatrix} \cos\phi & -\sin\phi & \beta \\ \sin\phi & \cos\phi & -\alpha \\ \alpha \cdot \sin\phi - \beta \cdot \cos\phi & \alpha \cdot \cos\phi + \beta \cdot \sin\phi & \cos\alpha \cdot \cos\beta \end{bmatrix} \cdot \begin{Bmatrix} x' \\ y' \\ z' \end{Bmatrix} + \begin{Bmatrix} \delta \cdot \cos(\phi+\theta) \\ \delta \cdot \sin(\phi+\theta) \\ z_l \end{Bmatrix} \tag{A.1}$$

Therefore, shaft displacements at the bearing locations (z'=a, L) for the coupled case, relative to the uncoupled static positions (Fig. 2), can be determined as,

$$\begin{aligned} x_1 &= \delta \cdot [\cos(\phi+\theta) - \cos\theta] + a \cdot [\beta - \beta_0] \\ y_1 &= \delta \cdot [\sin(\phi+\theta) - \sin\theta] - a \cdot [\alpha - \alpha_0] \\ x_2 &= \delta \cdot [\cos(\phi+\theta) - \cos\theta] + L \cdot [\beta - \beta_0] \\ y_2 &= \delta \cdot [\sin(\phi+\theta) - \sin\theta] - L \cdot [\alpha - \alpha_0] \end{aligned} \tag{A.2}$$

where α and β are determined from the system equations of motion (13).

The driven-rotor mass, m, located at distance h from the coupling, is offset from the shaft axis by an amount e and lies in the x–z plane at t^*=0, (Fig. 1c). Therefore mass displacement in the stationary x–y–z coordinate system is determined from Eq. (A.1) so that the mass translational velocities $\dot{x}_m$, $\dot{y}_m$ and $\dot{z}_m$ can be computed from

$$\begin{Bmatrix} \dot{x} \\ \dot{y} \\ \dot{z} \end{Bmatrix}_m = \frac{\mathrm{d}}{\mathrm{d}t} \begin{Bmatrix} x \\ y \\ z \end{Bmatrix}_m = \begin{Bmatrix} -e \cdot \dot{\phi} \cdot \sin\phi + \dot{\beta} \cdot h - \delta \cdot \dot{\phi} \cdot \sin(\phi+\theta) \\ e \cdot \dot{\phi} \cdot \cos\phi - \dot{\alpha} \cdot h + \delta \cdot \dot{\phi} \cdot \cos(\phi+\theta) \\ e \cdot (\alpha \cdot \dot{\phi} \cdot \cos\phi + \dot{\alpha} \cdot \sin\phi + \beta \cdot \dot{\phi} \cdot \sin\phi - \dot{\beta} \cdot \cos\phi) \\ -h(\dot{\beta} \cdot \sin\beta\cos\alpha + \dot{\alpha} \cdot \sin\alpha\cos\beta) + \dot{z}_l \end{Bmatrix} \tag{A.3}$$

Appendix B

B.1. System equations of motion

The full mass, stiffness, damping and force matrices for the derived system equations of motion (13) are as follows:

$$[M]=\begin{bmatrix} mh^2 & 0 & 0 & -m\cdot h\cdot[e\cos\phi+\delta\cos(\phi+\theta)] & m[e\sin\phi-h\alpha] \\ 0 & mh^2 & 0 & -m\cdot h\cdot[e\sin\phi+\delta\sin(\phi+\theta)] & -m[e\cos\phi+h\beta] \\ 0 & 0 & I_1 & 0 & 0 \\ -m\cdot h\cdot[e\cos\phi+\delta\cos(\phi+\theta)] & -m\cdot h\cdot[e\sin\phi+\delta\sin(\phi+\theta)] & 0 & I_2\cdot(\cos^2\alpha\cdot\cos^2\beta)+m\delta^2 & 0 \\ m[e\sin\phi-h\alpha] & -m[e\cos\phi+h\beta] & 0 & 0 & m \end{bmatrix} \tag{B.1}$$

$$[K]=\begin{bmatrix} k_y(a^2+L^2)+k_c\cdot[1+\sum_{i=1}^{i=N}a_i\cdot\cos(i\phi+\lambda_i)] & 0 & 0 & 0 & 0 \\ 0 & k_x(a^2+L^2)+k_c\cdot[1+\sum_{i=1}^{i=N}a_i\cdot\sin(i\phi+\lambda_i)] & 0 & 0 & 0 \\ 0 & 0 & k_t & -k_t\cos\alpha\cos\beta & 0 \\ 0 & 0 & -k_t\cos\alpha\cos\beta & k_t\cos^2\alpha\cos^2\beta & 0 \\ 0 & 0 & 0 & 0 & k_z \end{bmatrix} \tag{B.2}$$

$$[C]=\begin{bmatrix} C_y(a^2+L^2) & 0 & 0 & -C_y(a+L)\delta\cos(\phi+\theta)-C_y(a^2+L^2)\sin\beta & 0 \\ 0 & C_x(a^2+L^2) & 0 & -C_x(a+L)\delta\sin(\phi+\theta)+C_x(a^2+L^2)\sin\alpha & 0 \\ 0 & 0 & C_t & -C_t\cos\alpha\cos\beta & 0 \\ -C_y(a+L)\delta\cos(\phi+\theta)-C_y(a^2+L^2)\sin\beta & -C_x(a+L)\delta\sin(\phi+\theta)+C_x(a^2+L^2)\sin\alpha & -C_t\cos\alpha\cos\beta & C_t\cos^2\alpha\cos^2\beta+[C_y-C_x]\cdot\delta^2\cos(2\phi+2\theta)+[C_y-C_x]\cdot\delta^2 & 0 \\ 0 & 0 & 0 & 0 & C_z \end{bmatrix} \tag{B.3}$$

$$\{F\}=\begin{Bmatrix} k_y(a^2+L^2)\alpha_0-k_y(a+L)\delta\sin\theta+k_y(a+L)\delta\sin(\phi+\theta)-[k_c\cdot[1+\sum_{i=1}^{i=N}a_i\cdot\cos(i\phi+\lambda_i)]]\cdot\tau\cdot\cos\phi-mh\delta\dot\phi^2\cdot\sin(\phi+\theta)+mhe[\dot\alpha^2+\dot\beta^2-\dot\phi^2]\cdot\sin\phi-T_L\sin\beta+mhg \\ k_x(a^2+L^2)\cdot\beta_0+k_x(a+L)\cdot\delta\cos\theta-k_x(a+L)\cdot\delta\cos(\phi+\theta)-[k_c\cdot[1+\sum_{i=1}^{i=N}a_i\cdot\sin(i\phi+\lambda_i)]]\cdot\tau\cdot\sin\phi+mh\delta\dot\phi^2\cdot\cos(\phi+\theta)-mhe[\dot\alpha^2+\dot\beta^2-\dot\phi^2]\cdot\cos\phi+T_L\sin\alpha \\ T_i \\ [k_x-k_y]\cdot\delta^2\sin(2\phi+2\theta)-k_x\delta^2(2\sin(\phi+\theta)\cdot\cos\theta)+k_y\cdot\delta^2\cdot(2\cos(\phi+\theta)\cdot\sin\theta)-k_x\cdot(a+L)\cdot\delta\cdot\sin(\phi+\theta)\cdot(\beta_0-\beta)-k_y(a+L)\cdot\delta\cdot\cos(\phi+\theta)\cdot(\alpha_0-\alpha)-T_L\cos\alpha\cos\beta-mg[\delta\cdot\cos(\phi+\theta)+e\cos\phi] \\ mh(\ddot\alpha^2+\ddot\beta^2)-2\cdot me\dot\alpha\dot\phi\cos\phi-2\cdot me\dot\beta\dot\phi\sin\phi \end{Bmatrix} \tag{B.4}$$

B.2. Dimensionless equations of motion

Ignoring small second-order terms, including gravitational effects and assuming small angular displacements ($\sin\alpha=\alpha$; $\sin\beta=\beta$), the equations of motion (B.1)–(B.4) are non-dimensionalised by dividing through by $m\omega_{ny}^2L^2$ and defining dimensionless time $t^*=\omega_{ny}\cdot t$. Then,

$$[M^*]\{\ddot{q}^*\}+[C^*]\{\dot{q}^*\}+[K^*]\{q^*\}=\{F^*\} \tag{B.5}$$

and the dimensionless generalized coordinates are defined

$$\{q^*\}=\left\{\alpha,\beta,\psi,\phi,\frac{z_l}{L}\right\}^{\mathrm{T}}=\{\alpha^*,\beta^*,\psi^*,\phi^*,z_l^*\}^{\mathrm{T}} \tag{B.6}$$

$$\{\dot{q}^*\}=\left\{\frac{\dot{\alpha}}{\omega_{ny}},\frac{\dot{\beta}}{\omega_{ny}},\frac{\dot{\psi}}{\omega_{ny}},\frac{\dot{\phi}}{\omega_{ny}},\frac{\dot{z}_l}{\omega_{ny}L}\right\}^{\mathrm{T}}=\left\{\dot{\alpha}^*,\dot{\beta}^*,\dot{\psi}^*,\dot{\phi}^*,\dot{z}_l^*\right\}^{\mathrm{T}} \tag{B.7}$$

$$\{\ddot{q}^*\}=\left\{\frac{\ddot{\alpha}}{\omega_{ny}^2},\frac{\ddot{\beta}}{\omega_{ny}^2},\frac{\ddot{\psi}}{\omega_{ny}^2},\frac{\ddot{\phi}}{\omega_{ny}^2},\frac{\ddot{z}_l}{\omega_{ny}^2L}\right\}^{\mathrm{T}}=\left\{\ddot{\alpha}^*,\ddot{\beta}^*,\ddot{\psi}^*,\ddot{\phi}^*,\ddot{z}_l^*\right\}^{\mathrm{T}} \tag{B.8}$$

Note that all system natural frequencies are normalized with respect to the lateral frequency of the driven rotor in the y-direction, ω_{ny}. Other dimensionless parameters are defined in the nomenclature. The reduced dimensionless system matrices are,

Mass matrix

$$[M^*]=\begin{bmatrix} h^{*2} & 0 & 0 & -h^*\cdot[u\cos\phi+p\cos(\phi+\theta)] & [u\sin\phi-h^*\alpha] \\ 0 & h^{*2} & 0 & -h^*\cdot[u\sin\phi+p\sin(\phi+\theta)] & -[u\cos\phi+h^*\beta] \\ 0 & 0 & r_1^2 & 0 & 0 \\ -h^*\cdot[u\cos\phi+p\cos(\phi+\theta)] & -h^*\cdot[u\sin\phi+p\sin(\phi+\theta)] & 0 & r_2^2 & 0 \\ [u\sin\phi-h^*\alpha] & -[u\cos\phi+h^*\beta] & 0 & 0 & 1 \end{bmatrix} \tag{B.9}$$

Stiffness matrix

$$[K^*]=\begin{bmatrix} h^{*2}\left[\dfrac{(1+a^{*2}+k_{c\alpha}^*)}{(1+a^{*2}+k_c^*)}+(\dot{\alpha}^{*2}+\dot{\beta}^{*2})\right] & 0 & 0 & 0 & 0 \\ 0 & h^{*2}\left[\dfrac{k_1(1+a^{*2})+k_{c\beta}^*}{(1+a^{*2}+k_c^*)}+(\dot{\alpha}^{*2}+\dot{\beta}^{*2})\right] & 0 & 0 & 0 \\ 0 & 0 & f_t^2\cdot r_2^2 & -f_t^2\cdot r_2^2 & 0 \\ 0 & 0 & -f_t^2\cdot r_2^2 & f_t^2\cdot r_2^2 & 0 \\ 0 & 0 & 0 & 0 & f_z^2 \end{bmatrix} \tag{B.10}$$

Damping matrix

$$[C^*]=\begin{bmatrix} 2\cdot\zeta_y(1+a^{*2}) & 0 & 0 & 0 & 0 \\ 0 & 2\cdot f_x\zeta_x(1+a^{*2}) & 0 & 0 & 0 \\ 0 & 0 & 2\cdot r_2^2\cdot\zeta_t\cdot f_t & -2\cdot r_2^2\cdot\zeta_t\cdot f_t & 0 \\ 0 & 0 & -2\cdot r_2^2\cdot\zeta_t\cdot f_t & 2\cdot r_2^2\cdot\zeta_t\cdot f_t & 0 \\ 0 & 0 & 0 & 0 & 2\cdot f_z\cdot\zeta_z \end{bmatrix} \tag{B.11}$$

and the dimensionless force vector is

$$\{F^*\}=\begin{Bmatrix} \{A_1\cdot\alpha_0-A_2\cdot p\cdot\sin\theta\}+A_2\cdot p\cdot\sin(\phi+\theta)-A_3\cdot k_{c\alpha}^*\cdot\tau\cdot\cos\phi-h^*\dot{\phi}^{*2}\cdot[p\cdot\sin(\phi+\theta)]+h^*\cdot(\dot{\alpha}^{*2}+\dot{\beta}^{*2}-\dot{\phi}^{*2})\cdot u\cdot\sin\phi-\beta\cdot T_L^* \\ k_1\cdot\{A_1\cdot\beta_0+A_2\cdot p\cdot\cos\theta\}-k_1\cdot A_2\cdot p\cdot\cos(\phi+\theta)-A_3\cdot k_{c\beta}^*\cdot\tau\cdot\sin\phi+h^*\cdot\dot{\phi}^{*2}\cdot[p\cdot\cos(\phi+\theta)]-h^*\cdot(\dot{\alpha}^{*2}+\dot{\beta}^{*2}-\dot{\phi}^{*2})\cdot u\cdot\cos\phi+\alpha\cdot T_L^* \\ T_d^* \\ -A_3\cdot p^2\cdot\{[1-k_1]\cdot\sin(2(\phi+\theta))+2\cdot k_1\cdot\cos\theta\cdot\sin(\phi+\theta)\}-A_2\cdot p\cdot[k_1\cdot(\beta_0-\beta)\cdot\sin(\phi+\theta)+(\alpha_0-\alpha)\cdot\cos(\phi+\theta)]-T_L^*\cos\alpha\cdot\cos\beta \\ h^*(\dot{\alpha}^{*2}+\dot{\beta}^{*2}) \end{Bmatrix} \tag{B.12}$$

where A_1, A_2 and A_3 are constants determined by the driven shaft configuration and coupling relative-stiffness properties,

$$A_1=\frac{h^{*2}(1+a^{*2})}{(1+a^{*2}+k_c^*)};A_2=\frac{h^{*2}(1+a^*)}{(1+a^{*2}+k_c^*)};A_3=\frac{h^{*2}}{(1+a^{*2}+k_c^*)} \tag{B.13,14,15}$$

Appendix C

The nonlinear bearing forces are defined as,

$$F_{x1} = k_{nx} \cdot \text{sign}(x_1) \cdot |x_1|^{m_X}; F_{x2} = k_{nx} \cdot \text{sign}(x_2) \cdot |x_2|^{m_X} \quad \text{(C.1,2)}$$

$$F_{y1} = k_{ny} \cdot \text{sign}(y_1) \cdot |y_1|^{m_Y}; F_{y2} = k_{ny} \cdot \text{sign}(y_2) \cdot |y_2|^{m_Y} \quad \text{(C.3,4)}$$

where the parameters k_{nx}, m_x, k_{ny} and m_y define the magnitude and form of the bearing nonlinear stiffness in x and y directions, respectively. These nonlinear bearing forces produce bending moments, $M_{N\alpha}$ and $M_{N\beta}$, about the x and y axes, respectively.

$$M_{N\alpha} = k_{ny} \cdot \text{sign}(y_1) \cdot |y_1|^{m_y} \cdot a + k_{ny} \cdot \text{sign}(y_2) \cdot |y_2|^{m_Y} \cdot L \quad \text{(C.5)}$$

$$M_{N\beta} = -k_{nx} \cdot \text{sign}(x_1) \cdot |x_1|^{m_X} \cdot a - k_{nx} \cdot \text{sign}(x_2) \cdot |x_2|^{m_X} \cdot L \quad \text{(C.6)}$$

A torque, $M_{N\phi}$, is also created about the z-axis,

$$\begin{aligned} M_{N\phi} = {} & k_{nx} \cdot \{\text{sign}(x_1) \cdot |x_1|^{m_X} \cdot [\delta \cdot \sin(\phi+\theta) - a \cdot \alpha] + \text{sign}(x_2) \cdot |x_2|^{m_X} \cdot [\delta \cdot \sin(\phi+\theta) - L \cdot \alpha]\} \\ & -k_{ny} \cdot \{\text{sign}(y_1) \cdot |y_1|^{m_y} \cdot [\delta \cdot \cos(\phi+\theta) + a \cdot \beta] + \text{sign}(y_2) \cdot |y_2|^{m_Y} \cdot [\delta \cdot \cos(\phi+\theta) + L \cdot \beta]\} \end{aligned} \quad \text{(C.7)}$$

Substituting for x_1, x_2, y_1 and y_2 from Eqs. (A.2) into (C.5), (C.6) and (C.7) and converting to dimensionless form, as before, we obtain the nonlinear dimensionless generalized forces,

$$M^*_{N\alpha} = D_x\{\text{sign}(B_1) \cdot |B_1|^{m_y} \cdot a^* + \text{sign}(B_2) \cdot |B_2|^{m_Y}\} \quad \text{(C.8)}$$

$$M^*_{N\beta} = -D_y \cdot \{\text{sign}(B_3) \cdot |B_3|^{m_X} \cdot a^* + \text{sign}(B_4) \cdot |B_4|^{m_X}\} \quad \text{(C.9)}$$

$$\begin{aligned} M^*_{N\phi} = {} & D_x \cdot \{\text{sign}(B_3) \cdot |B_3|^{m_X} \cdot [p \cdot \sin(\phi+\theta) - a^* \cdot \alpha] + \text{sign}(B_4) \cdot |B_4|^{m_X} \cdot [p \cdot \sin(\phi+\theta) - \alpha]\} \\ & -D_y \cdot \{\text{sign}(B_1) \cdot |B_1|^{m_y} \cdot [p \cdot \cos(\phi+\theta) + a^* \cdot \beta] + \text{sign}(B_2) \cdot |B_2|^{m_Y} \cdot [p \cdot \cos(\phi+\theta) + \beta]\} \end{aligned} \quad \text{(C.10)}$$

where,

$$B_1 = a^* \cdot [\alpha_0 - \alpha] + p \cdot [\sin(\phi+\theta) - \sin\theta]; B_2 = [\alpha_0 - \alpha] + p \cdot [\sin(\phi+\theta) - \sin\theta]$$

$$B_3 = a^* \cdot [\beta - \beta_0] + p \cdot [\cos(\phi+\theta) - \cos\theta]; B_4 = [\beta - \beta_0] + p \cdot [\cos(\phi+\theta) - \cos\theta] \quad \text{(C.11)}$$

and

$$D_x = \frac{k^*_{nx} \cdot h^{*2}}{(1 + a^{*2} + k^*_{co})} = k^*_{nx} \cdot A_3, \text{where } k^*_{nx} = \frac{k_{nx}}{k_y} \cdot L^{(m_x - 1)} \quad \text{(C.12,13)}$$

$$D_y = \frac{k^*_{ny} \cdot h^{*2}}{(1 + a^{*2} + k^*_{co})} = k^*_{ny} \cdot A_3, \text{where } k^*_{ny} = \frac{k_{ny}}{k_y} \cdot L^{(m_y - 1)} \quad \text{(C.14,15)}$$

References

[1] J. Piotrowski, *Shaft Alignment Handbook*, 2ndsecond ed., Marcel Dekker Inc., New York, 1995.

[2] J. Piotrowski, "Why Shaft Misalignment Continuesshaft misalignment continues to Befudlebefudle and Undermine Evenundermine even the Best CBMbest cbm and Pro-Active Maintenance Programs", Proc. Of Thepro-active maintenance programs, *Proceedings of the Predictive Maintenance Technology National Conference*, Indianapolis, In 5: 18–23, DecDecember 3–6, 1996.

[3] C.B. Gibbons, Coupling *Misalignment Forces*, Proc.misalignment forces, *Proceedings of 5th Turbomachinery Symposium*, 1976, pp. 111–116.

[4] D.L. Dewell, L.D. Mitchell, Detection of a misaligned disk coupling using spectrum analysis, *Trans. actions of ASME, JnlJournal of Vibration, Acoustics, Stress and Reliability in Design* 106 (1984) 9–18.

[5] M. Xu, R.D. Marangoni, Flexible couplings: study and application, *Shock and Vibration Digest* 22 (9) (1990).

[6] M. Xu, R.D. Marangoni, Vibration analysis of a motor-flexible coupling-rotor system subject to misalignment and unbalance, part I: theoretical model and analysis, *JnlJournal of Sound and Vibration* 176 (5) (1994) 663–679.

[7] M. Xu, R.D. Marangoni, Vibration analysis of a motor-flexible coupling-rotor system subject to misalignment and unbalance, part II: experimental validation", *JnlJournal of Sound and Vibration* 176 (5) (1994) 663–691.

[8] A.S. Sekhar, B.S. Prabhu, Effects of coupling misalignment on vibrations of rotating machinery, *JnlJournal of Sound and Vibration* 185 (4) (1995) 655–671.

[9] R.A. Sreenivasa, A.S. Sekhar, Vibration *Analysis*analysis of *Rotor-Coupling-Bearing System*rotor-coupling-bearing system with *Misaligned Shafts*misaligned shafts, *ASME Paper 96-GT-12, Intl. Gas Turbine & Aeroengine Congress and Exhibition*, Birmingham, UK, 10–13 June, 1996.

[10] A.S. Sekhar, R.A. Sreenivasa, Crack versus misalignment in rotor-coupling-bearing-system, *Machine Vibration* 5 (1996) 179–188 Springer-Verlag London Limited.

[11] S. Prabhakar, A.S. Sekhar, A.R. Mohanty, Vibration analysis of a misaligned rotor-coupling-bearing system passing through the critical speed, *Proc. Instn. Mech. Engrs.eedings of the Institution of Mechanical Engineers* 215 (Part C) (2001).

[12] S. Arumugam, S. Swarnamani, B.S. Prabhu, Effects of coupling misalignment on the vibration characteristics of a two stage turbine rotor, *ASME Design Engineering Technical Conference* 3 (Part B) (1995).

[13] Y.S. Lee, C.W. Lee, Modelling and vibration analysis of misaligned rotor-ball bearing systems, *Jnl.Journal of Sound and Vibration* 224 (1) (1999) 17–32.

[14] C. Jackson, Back *To Fundamentals—Part*to fundamentals—part 5 *Preloads*preloads (Alignment), *Vibration Institute Mini Course Notes, 16th Annual Meeting*, Williamsburg, Virginia, 1992.

[15] M.A. Hili, T. Fakhfakh, L. Hammami, M. Haddar, Angular misalignment effect on the dynamic behavior of bearings, *Intl. Jnl.International Journal of Mechanical Engineering educationEducation* 34 (3) (2006) 183–193.
[16] K.M. Hussain, I. Redmond, Dynamic response of two rotors connected by rigid type mechanical coupling with parallel misalignment, *JnlJournal of Sound and Vibration* 249 (3) (2002) 483–498.
[17] A.W. Lees, Some *Studies*studies on *Misalignment*misalignment in *Rigidly Coupled Flexible Rotors*rigidly coupled flexible rotors, *7th IFToMM Conference on Rotor Dynamics*, Vienna, Austria, September 2006, pp. 25–28 Sept., 2006.
[18] A.W. Lees, Misalignment in *Rigidly Coupled Flexible Rotors*, Proc. Intl.rigidly coupled flexible rotors, *Proceedings of International Modal Analysis Conf.erence (IMAC) XXV*, Orlando, Florida, USA, 19–22 Feb.,ruary 2007.
[19] A.W. Lees, Misalignment in rigidly coupled rotors, *Jnl. OfJournal of Sound and Vibration* 305 (2007) 261–371.
[20] I. Redmond, Shaft *Misalignment*misalignment and *Vibration—A Model*, Proc. Intl.vibration—a model, *Proceedings of International Modal Analysis Conf.erence (IMAC) XXV*, Orlando, Florida, USA, 19–22 Feb.,ruary 2007.
[21] A.W. Lees, J.E.T. Penny, The *Development*development of *Harmonics*harmonics in *Rotor Misalignment*rotor misalignment, *Vibrations in Rotating Machinery, IMechE Conference*, Exeter, September 2008.